Atlantis Highlights in Engineering, volume 8
Proceedings of the International Renewable Energy Storage Conference 2021 (IRES 2021)

Experimental Investigation of the Cycle Stability of different Iron Oxide Composites for a Redox Hydrogen Storage Process

Lea Huber [1], Bernd Gamisch [1] and Belal Dawoud [1]*

[1]*Laboratory of Sorption Processes, Technical University of Applied Sciences Regensburg, Germany*
**Corresponding author. Email: belal.dawoud@oth-r.de*

ABSTRACT – A promising process to store hydrogen is the thermochemical storage based on the repeated reduction and oxidation (redox) of iron oxide or iron. This storage process is an intermittent, two-phase reaction, which takes place under atmospheric pressure in a hydrogen atmosphere during reduction (charging) or in a steam atmosphere during oxidization (discharging). The investigations have been carried out at two constant temperatures, namely 700°C and 800°C. During the storage phase, only iron exists inside the storage reactor - a fact that makes the redox system much safer, compared to hydrogen storage under pressure in a tank.

This work aims at studying the effect of adding different supporting materials upon producing the iron oxide storage composite samples on their thermochemical cycle stability. Furthermore, the influence of the temperature during the initial sintering process and the redox cycles on the reaction behavior of the iron oxide composites is investigated.

It turned out that pure iron oxide pellets have lost about 65% of their redox potential after only three cycles. Applying 10 wt.% of calcium oxide has improved the cycle stability of the iron oxide pellets to over nine cycles. After nine cycles, a loss of redox performance by less than 5% was observed. This has been attributed to the densification of the sample's outer surface, which is associated with slowing down the gas diffusion rate into/out of the investigated sample. In addition, reducing the temperature during the cycling (800°C to 700°C) and the sintering from 1100°C to 950°C has shown a positive effect on enhancing the cycle stability.

Keywords: Hydrogen Storage, Iron/Iron Oxide, Redox Reactions, Cycle Stability

1 INTRODUCTION

To achieve the climate targets of the Paris agreement [1], an increased use of renewable energy sources instead of fossil fuels for energy generation is necessary. However, renewable energies like solar and wind are subjected to strong daytime and weather related fluctuations. To maintain a secure energy supply mainly consisting of renewable energy and to avoid regulation of renewable energy plants, energy storage systems have gained an increased importance. Storage systems can provide a temporal balance between energy production and consumption. Accordingly, the power grid can be relieved and the regulation of renewable energy plants can be prevented. Regarding an energy supply mainly consisting of renewable sources, the demand of sufficient, affordable and safe storage capacities will increase. [2, 3]

Another key role in the energy transition will be the cross-sector energy supply [3]. Hydrogen, as a central energy carrier for renewable energies, has proven to be an ideal candidate for such sector coupling [4–6]. The excess electricity of renewables can be used to generate hydrogen by spiting water via electrolysis. In times with a high-energy demand, hydrogen can be converted into electricity and heat by a fuel cell or a combustion engine connected to a generator. Alternatively, the stored hydrogen can be utilized as an energy carrier for transport.

In previous research works, different technologies to improve the energy density and safety of hydrogen storages have been investigated and developed [4, 7]. These technologies can be classified into two main categories: physical and chemical systems. Physical storages include compressed and liquefied hydrogen as well as adsorption on solid materials. Currently, the most common way is to store hydrogen in a tank after compression or liquefaction. However, about 9% to 12% of the stored energy is needed for the compression of hydrogen to 300 or 700 bar, respectively [8]. The volumetric energy density increases from 780 to 1300 Wh/dm^3 upon increasing the storage pressure of hydrogen from 350 to 700 bar. Storing hydrogen in liquid form results in enhancing the storage density to 2300 Wh/dm^3. [9] However, the necessary cooling down to -253°C at about 1 bar results in a loss between 20% to 50% of the lower heating value of the stored hydrogen [10]. Additionally, the amount of stored hydrogen decreases through evaporation losses and boil-off effects, which take pace over time. [4, 11]

In a chemical storage process, in most cases, hydrogen is chemically bound into a liquid or a solid carrier material. Using liquid organic hydrogen carriers (LOHC), unsaturated organic compounds such as N-ethylcarbazole,

naphthalene and toluene can be utilized [4, 10, 12, 13]. At a temperature of typically up to 200°C and a pressure of about 50 bar, the catalytic hydrogenation of the LOHC material takes place (charging phase). During the endothermic dehydrogenation of the hydrogen rich LOHC material, the absorbed hydrogen can be released with the use of a catalyst. For the discarding process, a temperature up to 310°C and a slight overpressure is needed. [10] Positive aspects of LOHC systems are the flexibility upon transporting the liquid storage medium and the achievable storage capacity. A storage density of 5.8 wt.% is given upon using the carrier N-ethylcarbazole (H0-NEC). [4, 12, 14] The necessary purification process of the released hydrogen after the dehydrogenation is still a challenge facing LOHC systems [10].

A further storage principle is to apply metal hydride (Me_nH_{2m}) systems, which are based on a reversible chemical reaction (Eq. 1). The process depends on the prevailing temperature, pressure and hydrogen concentration. During the exothermic charging process, the absorption of hydrogen (H_2) into the existing metal lattice (Me) takes place. In the endothermic discharge (desorption) phase, the bonded hydrogen is released from the metal hydride. [15–17]

$$n\,\mathrm{Me} + m\,\mathrm{H_2} \rightleftharpoons \mathrm{Me}_n\mathrm{H}_{2m} \tag{1}$$

In particular, metal hydride storage systems prove to be promising due to the volumetric H_2 storage capacity and safety [18]. The obtainable storage density depends on the applied material and varies between 1.6-1.8 wt.% (AB5-type) and 13.5 wt.% for Lithium borohydride ($LiBH_4$ + SiO_2) [4]. Currently, one problem is the increasing system temperature due to the heat released during the absorption phase, which leads to a decreased storage capacity, unless the storage tank is additionally cooled. [4, 16]

Another chemical storage method is based on the repeated reduction and oxidation (redox) of metal oxide or metal, respectively. In this case, hydrogen is not chemically bound. Instead, it is used for the reduction of metal oxide (Me_nO_m) to pure metal (Me). In the same time, hydrogen is oxidized to steam (H_2O). The discharge phase is the reverse process in a steam atmosphere (see Eq. 2). [10, 19–21]

$$\mathrm{Me}_n\mathrm{O}_m + m\,\mathrm{H_2} \rightleftharpoons n\,\mathrm{Me} + m\,\mathrm{H_2O} \tag{2}$$

A challenge of this process is the high temperature in a range of about 500°C to 1000°C, depending on the used material and the charging / discharging rate [22, 23]. However, unlike LOHC and metal hydride systems, the most heat demand is required during the charging phase, when excess energy is available. Additionally, the released heat during the exothermic discharging phase (oxidation) can be utilized as an output energy to enhance the overall system efficiency [10]. Furthermore, the safety of the storage process represents a clear advantage. This is due to that only metal or metal oxide and no hydrogen is present during the storage phase. Furthermore, a high volumetric storage capacity can be reached. In [24], an energy storage density of 2800 Wh/(dm^3 bulk) for an iron based hydrogen systems was reported.

Currently, the kinetics of different solid metal materials such as Ce, Cu, Fe, Mn, Ni and W have been investigated during a repeated redox reaction [21–23, 25–31]. Research works in the field of solid oxide fuel cells (SOFC) and oxide ceramic batteries (ROB) [32–34] as well as chemical looping (CL) processes [35–37] have confirmed that the use of iron oxide as suitable carrier material is particularly advantageous. This is due to the thermodynamic behavior of the material, the cost-efficient production and the high availability [34, 38–40].

2 IRON REDOX PROCESS

The use of iron oxide goes back to the early 20^{th} century, where iron oxide was chosen as a solid carrier material for the production of hydrogen [41]. Instead of hydrogen, carbon monoxide (CO) was utilized for the reduction of iron oxide. Based on this method, one of the first large-scale process for the production of high-purity hydrogen was developed, the so-called "steam-iron" process [42, 43]. The temperature range was typically about 550°C to 900°C. Due to the oxidation of iron in a steam atmosphere, hydrogen was produced (see Eq. 3). The reduction of iron oxide takes place in a carbon monoxide (CO) or methane (CH_4) atmosphere (see Eq. 4, 5), which leads to the emission of carbon dioxide (CO_2). [42]

$$3\,\mathrm{Fe} + 4\,\mathrm{H_2O} \longrightarrow \mathrm{Fe_3O_4} + 4\,\mathrm{H_2} \tag{3}$$

$$\mathrm{Fe_3O_4} + 4\,\mathrm{CO} \longrightarrow 3\,\mathrm{Fe} + 4\,\mathrm{CO_2} \tag{4}$$

$$\mathrm{Fe_3O_4} + \mathrm{CH_4} \longrightarrow 3\,\mathrm{Fe} + 2\,\mathrm{H_2O} + \mathrm{CO_2} \tag{5}$$

2.1 Iron redox storage process

The iron redox storage process takes places at atmospheric pressure conditions. When hematite (Fe_2O_3) is used as the initial oxide, it is converted to magnetite in an upstream step (see Eq. 6) [44]. The stability range of hematite in relation to the prevailing temperatures (600°C to 800°C) and the oxygen partial pressure ($< 10^{-14}$ bar) prevents the formation of hematite again (cf. Fig. 1) [33, 45, 46].

$$3\,\mathrm{Fe_2O_3} + \mathrm{H_2} \longrightarrow 2\,\mathrm{Fe_3O_4} + \mathrm{H_2O} \tag{6}$$

Starting with Fe_3O_4 at a temperature in the range between 600°C and 800°C, the reversible storage process can be described by a two-stage reaction given in Equation 7 and 8 [40, 44, 46]. Due to crystal defects in the wuestite phase, the non-stoichiometric iron monoxide is called $Fe_{1-x}O$. Here, x expresses the deviation from stoichiometry. In the following, wuestite is simplified as ideal phase (FeO).

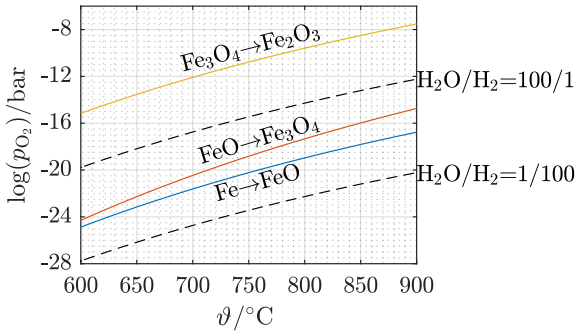

Figure 1 Equilibrium oxygen partial pressures of H_2O/H_2 mixtures as a function of temperature (Dashed lines) and dissociation pressures of the different iron oxide reactions (Solid lines); Calculated on the basis of [47].

$$Fe_3O_4 + H_2 \rightleftharpoons 3\,FeO + H_2O \quad (7)$$

$$FeO + H_2 \rightleftharpoons Fe + H_2O \quad (8)$$

During the charging phase, magnetite (Fe_3O_4) is first reduced to wuestite. In the second step, further reduction of wuestite to pure iron (Fe) takes place. Fig. 2 illustrates the reduction process, in the case of a porous structure. Starting from the gas phase (flow boundary layer), the gas transport takes places through the macro pores to the grain boundary (A). Through micro pores, the transport continues into the interior of the solid particles (B). Subsequently, at the gas/solid interface, oxygen is released from the crystal lattice and reacts with H_2 to steam (H_2O) (C). This leads to the migration of iron cations (Fe^{n+}) (solid-state diffusion, D). The transport of the generated steam takes place in a reverse order via micro and macro pores (E,F). [48, 49]

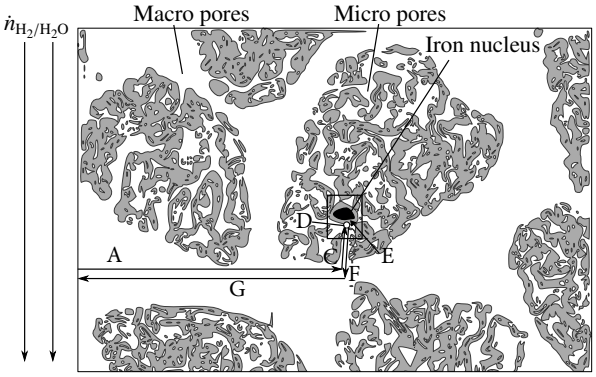

Figure 2 A schematic presentation of the reduction process: (A) Diffusion of H_2 through macro pores in the pellet, (B) Diffusion of H_2 through micro pores to reaction point, (C) Chemical reaction, (D) Movement of the iron cations Fe^{n+} and electrons e^- to the iron core, (E) Diffusion of H_2O through micro pores, (F) Diffusion of H_2O through macro pores (inspired by [48])

The discharge process is the reverse process, in which the pure iron oxidizes in a steam atmosphere first to wuestite and then to magnetite. [33]

Regarding the equilibrium condition (Eq. 9), the amount of storage or released oxygen (mass change during the redox process) is proportional to the amount of hydrogen or steam. Accordingly, the difference between the sample mass in the oxidized and reduced state represents a measure for the storage capacity.

$$O_2 + 2\,H_2 \rightleftharpoons 2\,H_2O \quad (9)$$

2.2 Aging process

The repeated redox reactions of pure iron oxide samples results in strong aging effects. In particular, the occurrence of aging effects leads to the agglomeration of iron particles and the increasing densification of the sample structure. The formation of a dense outer surface reduces the gas transport into the interior of the sample. This leads to a decrease in the reaction rate and can cause an incomplete conversion to iron or magnetite. [50–52]

N. Menzler et al. [34] have observed aging effects, which took place due to the repeated redox reaction when pure iron/iron oxide sample are used. After 5.5 redox cycles (reduced sate), it came out to an agglomerated structure and the formation of an outer dense iron layer. The investigations were carried out at a process temperature of 800°C and a reaction atmosphere of argon (Ar) with additionally ether hydrogen or steam (reduction: Ar with 2% H_2; oxidation: Ar with 2% H_2 and 7% H_2O).

The aging effects have been attributed to the high mobility and sintering tendency of iron cations during the redox process at a temperature range between 600°C and 800°C. Due to these effects, the available storage capacity decreases strongly with the number of cycles using pure iron/iron oxide samples. [33]

Despite the research carried out so far, the low cycle stability and, consequently, the short lifetime represents the biggest challenge of thermochemical hydrogen storage based on the redox process. In order to fulfill the requirements of an effective and stable storage material, a significant reduction of such aging effects deems quite necessary. This work aims, therefore at giving a hand towards enhancing the cycle stability by introducing different supporting materials upon producing the composite samples. Several redox cycles have been measured simultaneously to detect any aging effects. Moreover, microscopic images of the changed structure of the tested composites after cycling have been analyzed in order to explore the reason behind any obtained aging effect.

3 MATERIALS AND METHODS

Different supporting materials were added to an iron oxide powder with a particle size distribution of max. 60μm and a purity of 99.1% Fe_2O_3 (Linox GmBH).

3.1 Selection of supporting materials

A possible mitigation of aging effects, especially agglomeration of iron, has been achieved by adding suitable support materials. This could be proved in research works, which are dealing with the investigation of redox behavior of iron oxide materials for application in Solid Oxide Fuel Cell (SOFC), Rechargeable Oxide Battery (ROB) [32–34] or Chemical Looping (CL) processes [35–37].

In [35], different iron oxide samples with a supporting material amount of 15% and a diameter of about 4.5 mm were investigated at a temperature range of 700°C to 900°C. The comparatively best results were obtained in particular with CaO-rich samples. By comparing the mass change during oxidation and a temperature of 700°C, the reaction behavior of the CaO-rich sample (10%CaO, 5%Al_2O_3) was about four times faster than that of the sample without CaO (10% SiO_2, 5%Al_2O_3).

In a research work [35] focused on the investigation of iron oxide based oxygen storage materials for a SOFC, numerous support materials were tested with respect to their cycling stability over 20 redox cycles. The most promising results were obtained by adding CaO . In contrast, the use of other materials like TiO_2, CeO_2, Cr_2O_3, Mn_2O_3, MgO and CuO led to a strongly decreasing reaction behavior or even to a mixed crystals formation, which did not allow a repeated reduction of the sample. [34] In further work [35], the addition of pure SiO_2 and Al_2O_3 resulted in a negative influence on the redox reaction behavior. As a reason, the formation of inert mixed crystals ($SiFe_2O_4$ and $FeAl_2O_4$) was reported. By adding a support material consisting of a combination of SiO_2 and Al_2O_3 with CaO, an improvement in the cycling stability of the sample was achieved. This was attributed to a possible stabilizing effect of CaO through the formation of a dispersed structure, which mitigate the sintering effects of iron.

In this research work, CaO based supporting materials were chosen (cf. Tab. 1). These are a CaO powder with a purity of 96.8% and a CaO-rich Portland cement CEM1 42.5R with a clinker content of at least 95%. In addition, a fire cement with an composition of about 78% Al_2O and 21% CaO was selected. To keep the loss of active storage material as low as possible, the supporting materials were added with an amount of 10 wt.%.

Table 1 Applied supporting materials including the introduced abbreviations, chemical composition and manufacturer.

Name	Material	Composition	
Z	CEM1 42.5R	≥95% cement clinker	Heidelberg Cement
ZF	Secar 80	≥78.1% Al_2O_3 ≤21.4% CaO	Kerneos
CaO	nekafin0	96.8% CaO	Kalkfabrik Netstal

3.2 Manufacturing process and operation conditions

The manually produced samples have been sintered in an air atmosphere for a period of six hours. To investigate the influence of the temperature during the sintering process, some samples have been sintered at 950°C, while the others have been sintered at 1100°C. The initial mass of the investigated samples, after sintering, were about 1.4 g (see Tab. 2).

Table 2 List of parameters of produced storage samples with a support material content of 10 wt.%

Name	Support material	Initial weight (g)	Sinter temp. (°C)	Process temp. (°C)
Z	Z	1.49	950	800
ZF	ZF	1.36	950	800
CaO	CaO	1.36	950	800
CaO-02	CaO	1.38	1100	800
CaO-03	CaO	1.32	950	700
Fe_2O_3	-	1.41	950	700

In Fig. 3 the experimental setup is schematically illustrated. The reaction kinetics of the samples were investigated using a simultaneous thermogravimetric analyzer (STA 449 F3 Jupiter, Netzsch). Regarding the weight measuring, the accuracy of the STA device is $\pm 0.1\,\mu$g, while the accuracy for the sample temperature adjustment is about ± 0.3°C. To adjust different gas concentration (H_2, N_2), mass flow controllers (MFCs) were applied. The accuracy of one MCF is ± 0.5% regarding the gas flow in a range of 0 to 250 ml/min. For oxidation, the amount of steam was generated via an evaporator (DV2MK, ADROP) with an accuracy of $\pm$ 1% of the final value and a resolution of 0.1 g/h. To evacuate the experimental setup after each experiment as a safety precaution, a vacuum pump is used.

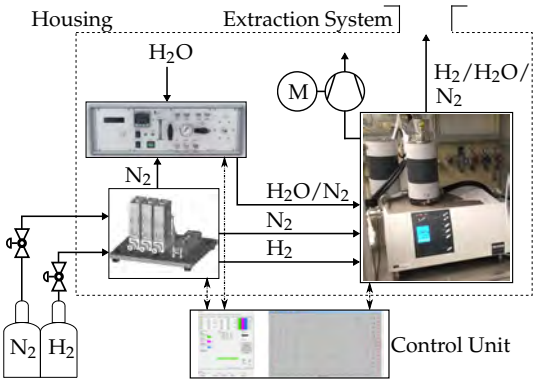

Figure 3 Schematic illustration of the setup for the experimental investigation of the reaction kinetics of storage samples [24].

The redox reactions have been carried out at 700°C or 800°C. The volume flow rate of the reacting gas amounts

to 250 ml/min. The vol.% of H_2 has been set to 50% during the reduction phase. During oxidation, the vol.% of H_2O has been set to 50%. In both phases, N_2 has been applied as a carrier gas.

4 RESULTS AND DISCUSSION

Regarding the prevailing process conditions, magnetite is the highest stable oxide. In the first redox cycle, the conversion of hematite to magnetite takes places. This leads to a reduction of the total sample mass (Tab. 2) of about 3%, according to Equation 6. With respect to the process conditions, hematite cannot be generated due to its unstable behavior (see Fig. 1). Thus, the relative mass of 100% represents the complete oxidation to Fe_3O_4.

4.1 Different supporting Materials

Fig. 4 depicts the reaction kinetics of different samples with the supporting materials (Z, ZF and CaO, cf. Tab. 2) during oxidation (discharging phase) at 800°C. Up to a relative mass of about 90% of the first oxidation cycle (C1), an approximately similar reaction behavior can be observed (Fig. 4 a). Regarding the complete conversion to Fe_3O_4, a masse change of about 24 wt.% was measured. The ZF-sample reaches its maximum in 19 min. In comparison, 6 and 8 minutes more are needed for the oxidation of the CaO- and Z-sample, respectively.

Fig. 4 b shows the reaction kinetics during the oxidation of the third and seventh redox cycles, respectively. Despite offering almost the same kinetics, the ZF-sample was mechanically damaged after three cycles. Consequently, no further investigations could be carried out. Concerning both the Z- and CaO-sample, a significant reduction in the reaction rates become obvious in the seventh cycles. After a reaction time of 100 min, a mass change of only 8 wt.% could be achieved using Z as a supporting material. In contrast, the CaO-sample could nearly reach its maximum (97%). In total, the loss of storage capacity is about 67% (Z- sample) and less than 3% (CaO- sample).

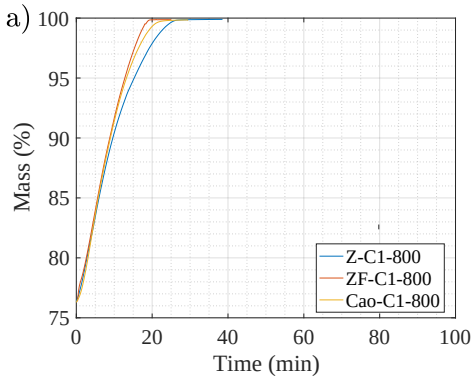

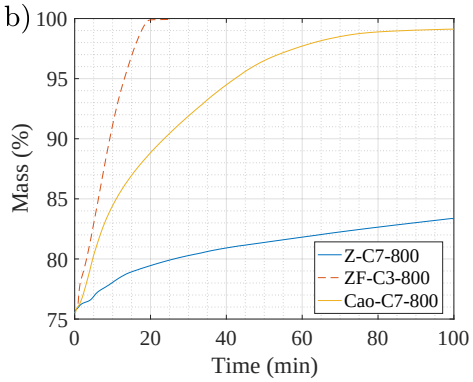

Figure 4 Mass change over the reaction time of the prepared samples with different supporting materials (Z: portland-cement; ZF: fire cement; CaO: pure calcium oxide) during the oxidation at 800°C. a) first cycle (C1); b) third (C3) or seventh cycle (C7)

The reason for the low mechanical stability of the ZF-sample could be the condensation of vacancies caused by the structural change of the crystal lattice during the redox reaction [45, 53]. In Fig. 5, the formation of a cavity between the interior and the rim can be seen, which causes low adhesion of the outer layer.

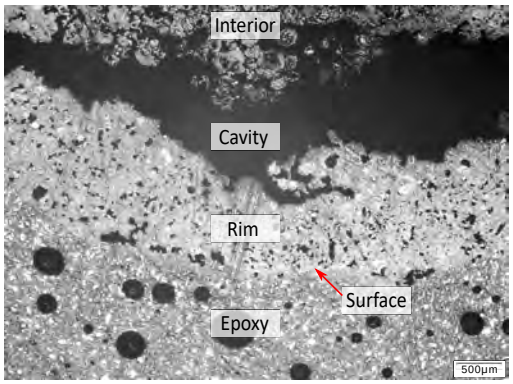

Figure 5 Microscopic image of an iron oxide sample with 10 wt.% ZF after the three redox cycles.

Regarding the Z- and CaO-sample, the change of the reaction kinetics with the number of redox cycles indicates that sintering effects occurred. Fig. 6 shows the microscopic structure of the outer layers and the sample surface after seven redox cycles. In both cases, a denser outer layer was formed. The densification of the sample structure leads to an impeded gas exchange (H_2, H_2O) into/out of the interior of the sample, which results in a slowdown of the reduction and oxidation process, respectively [34, 52]. In case of the Z-sample, the sharp decreases of the reaction rate and the storage capacity implies the formation of an strongly densified outer layer, which can be seen in Fig. 6 a. Furthermore, comparing the sample structure, a higher porosity can be observed by the CaO-sample. This correlates with the observed higher cycle stability.

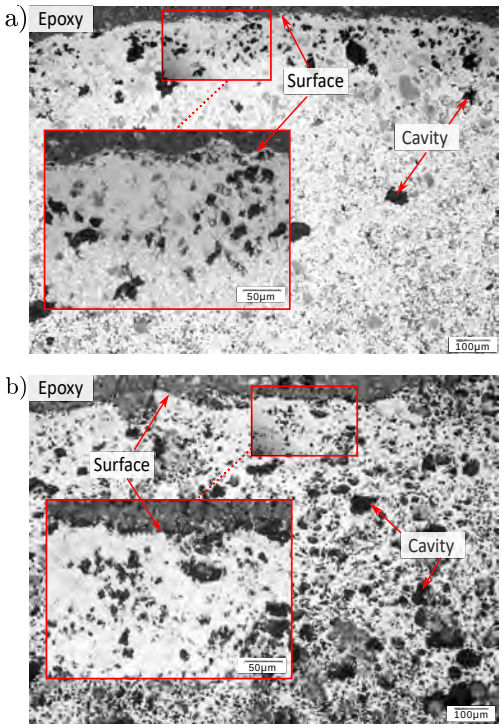

Figure 6 Microscopic images of the outer layers of an iron oxide sample after seven redox cycles at 800°C with 10 wt.% Z (a) and CaO (b) as supporting material.

Based on the obtained results, ZF and Z are not suitable to be applied as a support material in iron redox storage samples. However, compared to Z and ZF, CaO as supporting materiel showed promising results. This might be attributed to the mixed crystal formation of CaO and iron oxide, which leads to a higher stability, despite the significant increase in the required process time [36,44]. Due to the positive results, further investigations have been carried out only on iron oxide samples with 10 wt% CaO.

4.2 *Influence of the temperature during sintering*

In order to explore the effect of the temperature during the sintering process on the cycle stability, CaO-samples were sintered at 950°C (CaO-sample, S950) and 1100°C (CaO-01-sample, S1100), respectively. The redox cycles have been carried out at 800°C.

Fig. 7 shows the reaction kinetics of the samples during the first and second oxidation cycle. Compared to the CaO-sample, the first oxidation of the CaO-01-sample is already four times slower ($\Delta t_{C1-S950}$=25 min; $\Delta t_{C1-S1100}$=100 min). In the second cycle, a further decrease of the reaction rate can be observed. After 37 min, a mass change of only about 9 wt.% was reached, while in the first cycle, about 18 wt.% could be archived. Unlike this, the reaction behavior of the CaO-sample remained constant during the first two cycles.

The observed strong decrease in reaction rate of the sample sintered at 1100°C suggests that the increased

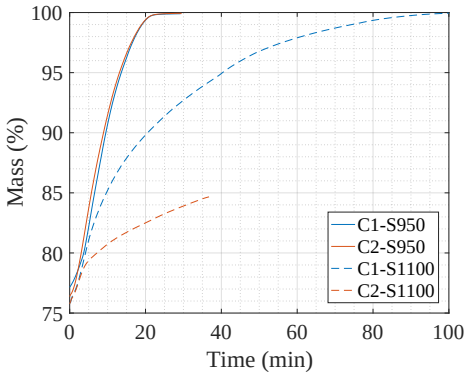

Figure 7 Mass change over reaction time of samples with 10 wt% CaO during the oxidation. First (C1) and second (C2) cycle at 800°C of samples sintered at 950°C (S950) or 1100°C (S1100).

temperature during the sintering process leads to a densification of the sample structure. This results in a reduced gas transport through the internal structure and a decreased conversion of iron to iron oxide, leading to a reduced cycle stability and storage capacity. [33, 34, 54]

4.3 *Influence of the process temperature*

The influence of the temperature during the redox cycles on the reaction kinetics has been studied. To this aim, CaO-samples were sintered at 950°C and investigated at a constant process temperature of 700°C (CaO-03sample; ro700) and 800°C (CaO-sample; ro800), respectively. In Fig. 8 the mass changes in the fifth and eighth oxidation cycle are depicted.

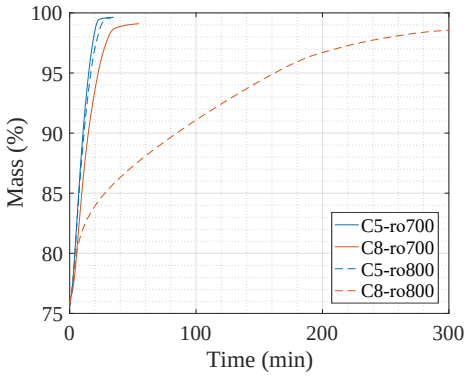

Figure 8 Mass change over reaction time of samples with 10 wt.% CaO and sintered at 950°C during the oxidation first (C1) and second (C2) oxidation at 700 or 800°C.

Regarding the fifth cycle, an approximately similar reaction kinetics is obtained. The averaged mass change is about 24 wt.% after 34 min. However, further cycling at a higher process temperature of 800°C causes a strong decrease in the kinetics. At a relative mass of about 80%, a clear decline of the reaction rate can be observed. As a

result, 300 minutes are needed to achieve a mass change of 23 wt.%. In comparison, at 700°C, almost the same mass change was obtained in 34 min. This indicates that a higher process temperature of 800°C during the cycling does stimulate the occurrence of effects.

4.4 Pure iron vs. CaO samples

Fig. 9 presents the reaction kinetics of storage samples with only pure iron oxide (Fig. 9 a) and 90% iron oxide and 10% CaO as supporting material (Fig. 9 b). Compared to the inertial sample weight, the mass loss in the first redox cycle is about 3.5 wt.% (pure iron oxide sample) and 3 wt.% (CaO-03-sample), respectively. This is due to the conversion of hematite to magnetite.

In case of pure iron oxide sample, a mass change of 27 wt.% can be measured in the first redox cycle. However, already in the second reduction cycle a strong decrease of the reaction rate can be observed (cf. Δt_{red1}=95 min, Δt_{red2}=864 min). Despite the nine times longer reaction time, a mass change of about 25 wt.% can be achieved during the second reduction and 21 wt.% during the second oxidation. In the subsequent third oxidation process, the mass change is further decreased to 9.5 wt.%. This represents already a loss of storage capacity of about 65%. These aging effects emerge mainly from the agglomeration of iron particles and the increasing densification of the sample structure, which includes the formation of a dense outer layer. [50–52]

Regarding the CaO-03-sample, the masse change in the first redox cycle is about 24 wt.%. The lower storage capacity (compared to 27 wt.% of pure iron oxide) is due to the amount of the support material. Over the first three cycles, an almost identical reaction behavior can be observed (cf. Fig. 9 b). The reaction time is about 85 min for the reduction and about 20 min for the oxidation.

Through the repeated redox reaction, a comparatively small decrease in the kinetics sets in. In the ninth cycle, a capacity loss of less than 5% is observed. Thereby, the reaction time has slowed down (Δt_{red9}=95 min, Δt_{ox9}=150 min). This indicates that the addition of 10 wt.% CaO has clearly improved the cycle stability but could not completely prevent the occurrence of aging effects.

5 CONCLUSION

In order to enhance the cycle stability of iron oxide samples for a hydrogen redox storage process, three various supporting materials (Portland cement (Z), fire cement (ZF) and calcium oxide (CaO)) were selected. Composite samples incorporating 10 wt.% of each supporting material with 90% of Fe_2O_3 have been prepared and cycled in a Thermo-Gravimetric Analyzer upon simultaneously measuring the reduction and oxidation kinetics in an atmosphere of H_2/N_2 during reduction and H_2O/N_2 during oxidation at different process temperatures. In addition, the influence of the sintering temperature on the cycle sta-

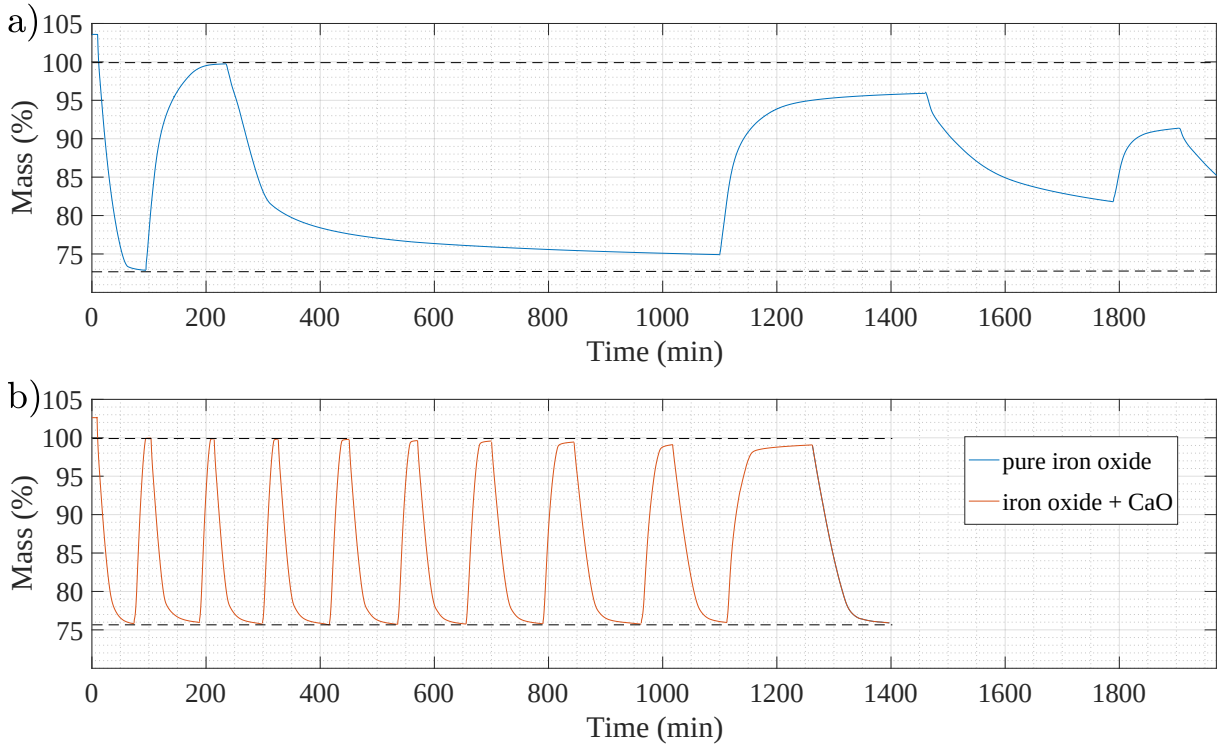

Figure 9 Mass change over reaction time of iron oxide samples with 0 wt% and 10 wt.% CaO (Fe_2O_3-,CaO-03-sample) during the reduction and oxidation at a process temperature of 700°C.

bility of the composites has been investigated. The structure of the investigated composite samples has been analyzed by a microscope to explore the reasons behind the low mechanical stability or the reduced reaction kinetics. The obtained results can be concluded as follows:

1. The cycle stability could be enhanced and the reaction kinetics could be maintained over more cycles by adding supporting materials, compared to the pure iron oxide samples.

2. CaO as a support material showed the best improvement concerning both cycle stability and reaction kinetics.

3. Reducing the sintering temperature from 1100°C to 950°C showed a significant improvement on both cycle stability and reaction kinetics of the investigated samples.

4. Reducing the process temperature from 800°C to 700°C resulted in another significant improvement of the composite stability of the investigated iron oxide composites based on CaO.

5. The reaction slowing down effect associated with the repeated redox cycles of the investigated samples could be attributed to the formation of a dense outer layer, which enhances the diffusion resistance of the reacting gases into/out of the samples.

6. Pure iron oxide samples lost about 23% and 65% of their redox storage capacity during the 2^{nd} and 3^{rd} redox cycles compared to the 1^{st} cycle. The needed cycle time is increased by a factor of 9 between the 1^{st} and 2^{nd} redox cycles.

7. Adding 10 wt.% of CaO as a supporting material to iron oxide has significantly improved the redox cycle stability but could not completely prevent the occurrence of aging effects. Accordingly more developments and investigations are needed to further enhance the cycle stability of the iron oxide composites.

ACKNOWLEDGMENT

The authors would like to acknowledge the funding by the Nagelschneider Foundation and the Regensburg Center of Energy and Resources (RCER). Moreover, the authors would like to acknowledge the project funding by the German Federal Ministries of Education and Research (BMBF) and of Economics and Energy (BMWi); project number 03SBE113D.

REFERENCES

[1] United Nations, "Paris Agreement," 2015.

[2] M. Aneke and M. Wang, "Energy storage technologies and real life applications – A state of the art review," *Applied Energy*, vol. 179, pp. 350–377, 2016.

[3] M. Sterner and I. Stadler, *Handbook of Energy Storage: Demand, Technologies, Integration*. Berlin and s.l.: Springer Berlin, 2018.

[4] I. Sreedhar, K. M. Kamani, B. M. Kamani, B. M. Reddy, and A. Venugopal, "A Bird's Eye view on process and engineering aspects of hydrogen storage," *Renewable and Sustainable Energy Reviews*, vol. 91, pp. 838–860, 2018.

[5] T. Veziroglu and F. Barbier, "HYDROGEN: THE WONDER FUEL," *International Journal of Hydrogen Energy*, no. 6, pp. 391–404, 1992.

[6] A. Sartbaeva, V. L. Kuznetsov, S. A. Wells, and P. P. Edwards, "Hydrogen nexus in a sustainable energy future," *Energy & Environmental Science*, vol. 1, no. 1, p. 79, 2008.

[7] S. Niaz, T. Manzoor, and A. H. Pandith, "Hydrogen storage: Materials, methods and perspectives," *Renewable and Sustainable Energy Reviews*, vol. 50, no. 7, pp. 457–469, 2015.

[8] K. Kunze and O. Kircher, "CRYO-COMPRESSED HYDROGEN STORAGE," 2012. [Online]. Available: https://docplayer.net/53367956-Cryo-compressed-hydrogen-storage.html

[9] H. Eichlseder and M. Klell, *Wasserstoff in der Fahrzeugtechnik*. Wiesbaden: Vieweg+Teubner, 2010.

[10] K. Müller, "Technologies for the Storage of Hydrogen: Part 1: Hydrogen Storage in the Narrower Sense," 2019.

[11] A. Godula-Jopek, W. Jehle, and J. Wellnitz, Eds., *Hydrogen Storage Technologies*. Weinheim, Germany: Wiley-VCH Verlag GmbH & Co. KGaA, 2012.

[12] M. Niermann, A. Beckendorff, M. Kaltschmitt, and K. Bonhoff, "Liquid Organic Hydrogen Carrier (LOHC) – Assessment based on chemical and economic properties," *International Journal of Hydrogen Energy*, vol. 44, no. 13, pp. 6631–6654, 2019.

[13] R. Aslam, M. Minceva, K. Müller, and W. Arlt, "Development of a liquid chromatographic method for the separation of a liquid organic hydrogen carrier mixture," *Separation and Purification Technology*, vol. 163, pp. 140–144, 2016.

[14] C. Gleichweit, M. Amende, S. Schernich, W. Zhao, M. P. A. Lorenz, O. Höfert, N. Brückner, P. Wasserscheid, J. Libuda, H.-P. Steinrück, and C. Papp, "Dehydrogenation of dodecahydro-N-ethylcarbazole on Pt(111)," *ChemSusChem*, vol. 6, no. 6, pp. 974–977, 2013.

[15] M. V. Lototskyy, V. A. Yartys, B. G. Pollet, and R. C. Bowman, "Metal hydride hydrogen compressors: A review," *International Journal of Hydrogen Energy*, vol. 39, no. 11, pp. 5818–5851, 2014.

[16] U. Eberle, M. Felderhoff, and F. Schüth, "Chemical and physical solutions for hydrogen storage," *Angewandte Chemie (International ed. in English)*, vol. 48, no. 36, pp. 6608–6630, 2009.

[17] M. Latroche, "Structural and thermodynamic properties of metallic hydrides used for energy storage," *Journal of Physics and Chemistry of Solids*, vol. 65, no. 2-3, pp. 517–522, 2004.

[18] M. Lototskyy, I. Tolj, M. W. Davids, P. Bujlo, F. Smith, and B. G. Pollet, ""Distributed hybrid" MH–CGH2 system for hydrogen storage and its supply to LT PEMFC power modules," *Journal of Alloys and Compounds*, vol. 645, pp. S329–S333, 2015.

[19] E. Lorente, J. A. Peña, and J. Herguido, "Cycle behaviour of iron ores in the steam-iron process," *International Journal of Hydrogen Energy*, vol. 36, no. 12, pp. 7043–7050, 2011. [Online]. Available: http://dx.doi.org/10.1016/j.ijhydene.2011.03.069

[20] C. M. Berger, A. Mahmoud, R. P. Hermann, W. Braun, E. Yazhenskikh, Y. J. Sohn, N. H. Menzler, O. Guillon, and M. Bram, "Calcium-Iron Oxide as Energy Storage Medium in Rechargeable Oxide Batteries," *Journal of the American Ceramic Society*, vol. 99, no. 12, pp. 4083–4092, 2016. [Online]. Available: http://dx.doi.org/10.1111/jace.14439

[21] M. Thaler and V. Hacker, "Storage and separation of hydrogen with the metal steam process," *International Journal of Hydrogen Energy*, vol. 37, no. 3, pp. 2800–2806, 2012. [Online]. Available: http://dx.doi.org/10.1016/j.ijhydene.2011.06.119

[22] T. Kodama, H. Ohtake, S. Matsumoto, A. Aoki, T. Shimizu, and Y. Kitayama, "Thermochemical methane reforming using a reactive WO_3/W redox system," *Energy*, vol. 25, no. 5, pp. 411–425, 2000.

[23] K. GO, S. SON, and S. KIM, "Reaction kinetics of reduction and oxidation of metal oxides for hydrogen production," *International Journal of Hydrogen Energy*, vol. 33, no. 21, pp. 5986–5995, 2008.

[24] B. Gamisch, M. Gaderer, and B. Dawoud, "On the Development of Thermochemical Hydrogen Storage; An Experimental Study of the Kinetics of the Redox Reactions under Different Operating Conditions," *Applied Sciences*, vol. 11, no. 4, p. 1623, 2021.

[25] A. Sim, N. W. Can, and D. L. Trimm, "Ceria–zirconia stabilised tungsten oxides for the production of hydrogen by the methane–water redox cycle," *International Journal of Hydrogen Energy*, vol. 17, no. 35, pp. 8953–8961, 2010.

[26] M. Forster, "Theoretical investigation of the system SnO_x/Sn for the thermochemical storage of solar energy," *Energy*, vol. 29, no. 5-6, pp. 789–799, 2004.

[27] T. Kodama, T. Shimizu, T. Satoh, M. Nakata, and K.-I. Shimizu, "Stepwise production of CO-rich syngas and hydrogen via solar methane reforming by using a Ni(II)–ferrite redox system," *Solar Energy*, vol. 73, no. 5, pp. 363–374, 2002.

[28] X. Zhu, H. Wang, Y. Wei, K. Li, and X. Cheng, "Hydrogen and syngas production from two-step steam reforming of methane using CeO_2 as oxygen carrier," *Journal of Natural Gas Chemistry*, vol. 20, no. 3, pp. 281–286, 2011.

[29] K. Otsuka, Y. Wang, E. Sunada, and I. Yamanaka, "Direct Partial Oxidation of Methane to Synthesis Gas by Cerium Oxide," *JOURNAL OF CATALYSIS*, no. 175, pp. 152–160, 1998.

[30] K. Otsuka, Y. Wang, and M. Nakamura, "Direct conversion of methane to synthesis gas through gas–solid reaction using CeO_2–ZrO_2 solid solution at moderate temperature," *Applied Catalysis A: General*, vol. 183, no. 2, pp. 317–324, 1999.

[31] X. Zhu, Y. Wei, H. Wang, and K. Li, "Ce–Fe oxygen carriers for chemical-looping steam methane reforming," *International Journal of Hydrogen Energy*, vol. 38, no. 11, pp. 4492–4501, 2013.

[32] C. M. Berger, "Sauerstoffspeicher für die oxidkeramische Batterie: Herstellung, Charakterisierung und Betriebsverhalten," Dissertation, Ruhr-Universität Bochum, Bochum, 2016.

[33] W. Braun, "Ermittlung thermochemischer und kinetischer Daten an Speichermaterialien zur Verwendung in einer oxidkeramischen Batterie," Dissertation, Rheinisch-Westfälischen Technischen Hochschule Aachen, 2017, forschungszentrum Jülich GmbH.

[34] N. H. Menzler, A. Hospach, L. Niewolak, M. Bram, O. Tokariev, C. Berger, P. Orzessek, W. J. Quadakkers, Q. Fang, and H. P. Buchkremer,

"Power-To-Storage - The Use of an Anode-Supported Solid Oxide Fuel Cell as a High-Temperature Battery," *ECS Transactions*, vol. 57, no. 1, pp. 255–267, 2013.

[35] G. Voitic and V. Hacker, "Recent advancements in chemical looping water splitting for the production of hydrogen," *RSC Advances*, vol. 6, no. 100, pp. 98 267–98 296, 2016.

[36] M. Ismail, W. Liu, and S. A. Scott, "The performance of Fe_2O_3-CaO Oxygen Carriers and the Interaction of Iron Oxides with CaO during Chemical Looping Combustion and H_2 production," *Energy Procedia*, vol. 63, pp. 87–97, 2014.

[37] W. Liu, J. Y. Lim, M. A. Saucedo, A. N. Hayhurst, S. A. Scott, and J. S. Dennis, "Kinetics of the reduction of wüstite by hydrogen and carbon monoxide for the chemical looping production of hydrogen," *Chemical Engineering Science*, vol. 120, pp. 149–166, 2014.

[38] V. Hacker, R. Fankhauser, G. Faleschini, H. Fuchs, K. Friedrich, M. Muhr, and K. Kordesch, "Hydrogen production by steam-iron process," *Journal of Power Sources*, vol. 86, no. 1-2, pp. 531–535, 2000.

[39] A. Pineau, N. Kanari, and I. Gaballah, "Kinetics of reduction of iron oxides by H_2: Part II. Low temperature reduction of magnetite," *Thermochimica Acta*, vol. 456, pp. 75–88, 2007.

[40] H. Chen, Z. Zheng, Z. Chen, and X. T. Bi, "Reduction of hematite (Fe_2O_3) to metallic iron (Fe) by CO in a micro fluidized bed reaction analyzer: A multistep kinetics study," *Powder Technology*, vol. 316, pp. 410–420, 2017.

[41] M. Anton, "Process of producing hydrogen," Patent US971 206 (A), 1908.

[42] H. Jack, L. J. James, C. S. Frank, JR, and B. T. Paul, "Production of hydrogen via the steam-iron process utilizing dual solids recycle," Patent US3 442 619 (A), 1969.

[43] M. Rydén and M. Arjmand, "Continuous hydrogen production via the steam–iron reaction by chemical looping in a circulating fluidized-bed reactor," *International Journal of Hydrogen Energy*, vol. 37, no. 6, pp. 4843–4854, 2012.

[44] W. K. Jozwiak, E. Kaczmarek, T. P. Maniecki, W. Ignaczak, and W. Maniukiewicz, "Reduction behavior of iron oxides in hydrogen and carbon monoxide atmospheres," *Applied Catalysis A: General*, vol. 326, no. 1, pp. 17–27, 2007.

[45] T. E. Mitchell, D. A. Voss, and E. P. Butler, "The observation of stress effects during the high temperature oxidation of iron," *Journal of Materials Science*, vol. 17, no. 6, pp. 1825–1833, 1982.

[46] A. Pineau, N. Kanari, and I. Gaballah, "Kinetics of reduction of iron oxides by H_2," *Thermochimica Acta*, vol. 447, pp. 89–100, 2006.

[47] D. J. Young, *High Temperature Oxidation and Corrosion of Metals*, 2nd ed. Amsterdam and Boston and Heidelberg and London: Elsevier, 2016.

[48] L. Bogdandy and H. J. Engell, *Die Reduktion der Eisenerze: Wissenschaftliche Grundlagen und technische Durchführung*. Berlin, Heidelberg: Springer Berlin Heidelberg, 1967.

[49] Q. T. Tsay, W. H. Ray, and J. Szekely, "The modeling of hematite reduction with hydrogen plus carbon monoxide mixtures: Part I. The behavior of single pellets," *AIChE Journal*, vol. 22, no. 6, pp. 1064–1072, 1976.

[50] S. P. Trushenski, K. Li, and W. O. Philbrook, "Non-Topochemical reduction of iron oxides," *Metallurgical Transactions*, vol. 5, no. 5, pp. 1149–1158, 1974.

[51] Z. Chen, J. Dang, X. Hu, and H. Yan, "Reduction Kinetics of Hematite Powder in Hydrogen Atmosphere at Moderate Temperatures," *Metals*, vol. 8, no. 10, p. 751, 2018.

[52] C. M. Berger, O. Tokariev, P. Orzessek, A. Hospach, Q. Fang, M. Bram, W. J. Quadakkers, N. H. Menzler, and H. P. Buchkremer, "Development of storage materials for high-temperature rechargeable oxide batteries," *Journal of Energy Storage*, vol. 1, pp. 54–64, 2015.

[53] H. J. Maier, T. Niendorf, and R. Bürgel, *Handbuch Hochtemperatur-Werkstofftechnik: Grundlagen, Werkstoffbeanspruchungen, Hochtemperaturlegierungen und -beschichtungen*, 6th ed., 2019.

[54] A. A. El-Geassy, "Gaseous reduction of Fe_2O_3 compacts at 600 to 1050°C," *Journal of Materials Science*, vol. 21, no. 11, pp. 3889–3900, 1986.